



Effects of thermal cycling on phenylethynyl-terminated PMDA-type asymmetric polyimide composites

High Performance Polymers
2019, Vol. 31(7) 861–871
© The Author(s) 2018
Article reuse guidelines:
sagepub.com/journals-permissions
DOI: 10.1177/0954008318804046
journals.sagepub.com/home/hip



Yixiang Zhang¹ , Masahiko Miyauchi² and Steven Nutt¹

Abstract

The effects of thermal cycling on a polymerized monomeric reactant (PMR) type polyimide (TriA X) reinforced with carbon fibers were investigated. Composite specimens were subjected to 2000 thermal cycles between -54°C and 232°C . At 400-cycle intervals, laminates were inspected for microcracks, and glass transition temperature (T_g) and short-beam shear (SBS) strength were measured. The composites did not exhibit microcracks after thermal cycling, although after 2000 thermal cycles, mechanical properties of the matrix declined slightly. The matrix degradation decreased the resistance to microcracking upon further loading. No effects of thermal oxidative aging were observed from thermal cycling, and thermally driven fatigue and creep were identified as the primary and secondary factors inducing mechanical degradation of the matrix. T_g of the composites exhibited no change after 2000 cycles, while the SBS strength decreased slightly (3–9%). The results highlight the potential for use of TriA X composites as long-term structural components in high-temperature service environments.

Keywords

Creep, microcracking, composite, polyimide, thermal cycling, thermal stress, thermally driven fatigue

Introduction

The volumetric shrinkage mismatch between a polymer matrix and carbon fibers generates thermal stress in composites during cooling. Thermally induced tensile stress on laminae can cause transverse microcracks, thereby decreasing mechanical performance and, in extreme cases, cause material failure.^{1,2} Damage introduced by thermal stress is a major concern in high-temperature polymer composites, because the composites are processed at high temperatures and experience a wide range of temperatures during service. In this work, thermal cycling tests were performed on a new polyimide–matrix composite to investigate the effects of thermal cycling on the mechanical performance and service life of the composites.

The cure process of thermoset prepreg creates three types of strain: chemical cure shrinkage, thermal shrinkage, and tool-part interaction.^{3,4} Tool-part interaction can be avoided simply by using release films between prepreg and tools. Second, the stress introduced by cure shrinkage is usually negligible if the cure temperature is greater than the glass transition temperature (T_g), because the curing resin is in a rubbery state with short relaxation time, high chain mobility, and low stiffness.⁵ Finally, the stress

generated by cure shrinkage is typically released during cure. Thus, it is generally assumed that composites are in a stress-free state during cure above T_g .^{6,7} After cure, the polymer matrix is vitrified and bonded to the fibers. Coefficients of thermal expansion (CTEs) of polymers generally are much greater than those of carbon fibers. Thus, volume change mismatch during cooling induces compressive stress in fibers and tensile stress in the matrix.¹ In laminates, the mismatch in properties between laminae of different orientations results in interlaminar stress.⁸ The longitudinal direction (0°) of a lamina has much lower CTE than the transverse direction (90°), and thus 90° plies

¹ Department of Chemical Engineering and Materials Science, University of Southern California, Los Angeles, CA, USA

² Kaneka U.S. Material Research Center, Kaneka Americas Holding, College Station, TX, USA

Corresponding author:

Yixiang Zhang, Department of Chemical Engineering and Materials Science, University of Southern California, 3651 Watt Way, Los Angeles, CA 90089, USA.
Email: zhangyix@usc.edu

induce tensile interlaminar stress on the adjacent 0° plies during cooling.^{1,9}

The thermal stress induced during laminate cooling is proportional to the temperature change (ΔT) from the cure temperature. The lower the minimum service temperature of a composite, the greater the thermal stress generated. When a composite is cycled between two temperatures, the composite experiences cyclic thermal stress. Thus, thermal cycling is equivalent to a form of thermally driven fatigue on each lamina.¹ Thermal stress can cause severe damage to composites. When the thermally induced stress exceeds the transverse tensile strength of a lamina, transverse microcracks can develop, and when thermal stress is greater than the interlaminar strength, delamination occurs.⁸

Polyimide-matrix composites are especially susceptible to defects induced by temperature variations during processing and service because of the high process temperatures and the brittle nature. Microcracking and mechanical degradation induced by temperature fluctuation have been reported for PMR-15 and other polyimide composites. For example, extensive microcracking in PMR-15 composites was reported in thermal cycling tests between -18°C and 232°C and between -156°C and 316°C .^{8,10} Thermal cycling (1500 cycles) between -54°C and 232°C of PMR-15 composites decreased both compressive strength and interlaminar shear strength by approximately 60%.¹¹ Indeed, some polyimide composites crack during processing. For example, PMR-II-50 polyimide composites microcracked upon cooling from 371°C (cure temperature) to room temperature during processing, and additional thermal cycling between room temperature and 316°C proliferated the microcracking.¹² Microcracks were also reported in thermal cycling tests of thermoplastic polyimide composites, specifically thermal cycling (-54°C and 177°C) of IM7/PIXA and IM7/K3B.¹³ Previous study has suggested that increased matrix strength reportedly increases composite resistance to thermal cycling, reducing microcracking.¹¹ Nevertheless, microcracking is a persistent problem for polyimide composites, because microcracks not only decrease mechanical performance but also accelerate degradation reactions, particularly thermal oxidation.¹⁴ Thus, microcracking resistance to thermal cycling is a critical performance metric for polyimide composites.

The present work describes a new polyimide with greater resistance to thermal cycling-induced microcracking compared to conventional polyimide composites. TriA X is a polymerized monomeric reactant (PMR) type polyimide derived from pyromellitic dianhydride (PMDA), 2-phenyl-4,4'-diaminodiphenyl ether (p-ODA), and 4-phenylethynylphthalic anhydride (PEPA). The term "TriA X" embodies the characteristics of the polymer molecules: *amorphous*, *asymmetric*, *addition-type*, and *cross-linked* (\times). TriA X features an asymmetric, irregular, and nonplanar backbone structure, resulting in an amorphous structure and greater toughness and ductility than

conventional polyimides (e.g. $\epsilon_b = 15.1\%$ at room temperature).¹⁵ For this work, we selected a TriA X polyimide system with a 3942-g mol^{-1} imide oligomer ($n = 7$). Conditioning up to 2000 thermal cycles between -54°C and 232°C was performed on 8-harness satin (8HS) T650-35 carbon fiber laminates produced with $[0/+45/-45/90]_s$ and $[0]_8$ layup sequences to investigate effects of thermal cycling. Thermomechanical analysis after conditioning indicated that thermal cycling did not produce microcracks, but indirectly decreased the resistance to microcracking because of matrix degradation. The matrix degradation was shown to arise primarily from thermally driven fatigue, while local creep was a possible secondary effect. Thermal cycling caused no decrease in T_g , and retention of short-beam shear (SBS) strength was $>90\%$, even after 2000 thermal cycles. The high stability of the polyimide composites upon thermal cycling was attributed to the high tensile strength and thermal oxidative stability of the matrix.

Thermal stress analysis

Material properties

CTE and Young's modulus of fiber and matrix are essential for the calculation of thermal stress in the composites during thermal cycling. Carbon fibers are thermally and dimensionally stable and, thus, the CTE and Young's modulus of T650-35 fiber are assumed to be constant in the temperature range from -54°C to 371°C (cure temperature of the composites). The properties of T650-35 fiber are taken from reported values, where Young's modulus = 241 GPa and $\text{CTE} = -0.5 \times 10^{-6}^\circ\text{C}^{-1}$.¹⁶

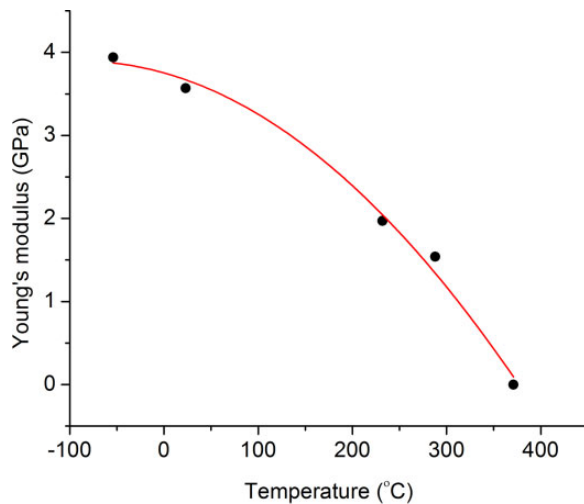
The values of CTE and Young's modulus for TriA X are functions of temperature. The CTE values of the polymer were measured in different temperature ranges using a thermomechanical analyzer (TMA; Q400, TA Instruments, New Castle, DE, USA) and are listed in Table 1. The measurement was carried out with a static force of 0.02 N from -55°C to 400°C at a ramp rate of 5°C min^{-1} under a nitrogen flow of 50.0 ml min^{-1} . The TMA was calibrated with a standard aluminium reference from -55°C to 400°C using the same parameters described above, and the calibration coefficient was determined according to ASTM E2113.¹⁷ The CTE of the polymer was calculated in accordance with ASTM E831.¹⁸

Young's modulus values are shown in Figure 1. The modulus values (black dots in Figure 1) at -54°C , 23°C , 232°C , and 288°C were measured from tensile tests.¹⁵ T_g of T650-35 8HS composites is 356°C , lower than the cure temperature (371°C). The stiffness of polymers above T_g is much less than that in the vitrified state. Thus, the Young's modulus of the polymer at 371°C is assumed to be zero. A second-order polynomial fitting curve of Young's modulus versus temperature (red line in Figure 1) was constructed based on the measured and assumed values

Table I. CTE of TriA X.

T (°C)	CTE ($10^{-6} \text{ } ^\circ\text{C}^{-1}$)
−54 to −25	36.6
−25 to 25	43.5
25 to 75	48.7
75 to 125	64.6
125 to 175	67.0
175 to 225	65.7
225 to 275	68.0
275 to 325	97.6
325 to 355	323.7
355 to 371	217.7

CTE: coefficient of thermal expansion.

**Figure 1.** Young's modulus of neat TriA X.

of modulus. The fitting curve is described by equation (1) with a $R^2 = 0.99$, indicating accurate fitting.

$$E_M = -1.8 \times 10^{-5} T^2 - 0.00319T + 3.753 \quad (1)$$

Thermal stress calculation

Thermal stress in T650-35 8HS composites was calculated to estimate the magnitude relative to material strength upon exposure to cyclic temperatures. In 0/90/0 cross-ply laminates fabricated with unidirectional plies, the CTE and elastic modulus mismatch between 0° plies (fiber direction, low CTE, and high modulus) and 90° plies (matrix direction, high CTE, and low modulus) generates transverse tensile stress on 90° plies during cooling after cure, and the stress can be determined by thermoelastic calculation.⁹ In T650-35 8HS composites, however, the shape of individual fiber tows in the cross-ply (non-crimp) region could not be distinguished after compression molding, while fill yarns occupied the entire area between warp yarns. Thus, the fill yarns in the cross-ply

region were considered as a 90° unidirectional ply with a 0° unidirectional ply (warp yarns) on each side. Consequently, the transverse thermal stress (σ) in the fill yarns of the cross-ply region was estimated by thermoelastic calculation, described by equation (2)^{1,9} and explained below. In this work, only the thermal stress in [0]_g layup was determined, because the orientation mismatch in cross-ply layup is the greatest for this case, and hence will produce the greatest thermal stress.

The modulus and CTE of unidirectional T650-35 composites were determined by assuming that the longitudinal and transverse properties of T650-35/TriA X were equal to the longitudinal properties of T650-35 fibers and the properties of neat TriA X, respectively. The property mismatch between longitudinal and transverse orientations of a unidirectional composite is less than that between fibers and matrix. Thus, this assumption will present an upper bound of thermal stress. In equation (2), α and E are CTE and Young's modulus, respectively, while the subscripts M and F represent "Matrix" and "Fiber," respectively.

$$\sigma = \sum \int_T^{371^\circ\text{C}} \frac{(\alpha_M - \alpha_F) E_F E_M}{E_F + E_M} dT \quad (2)$$

Because T650-35 8HS laminates were cured above T_g , during cure, polymer chains were in a rubbery state with high mobility and short relaxation time, allowing relaxation of stress induced by cure shrinkage.⁵⁻⁷ Thus, the internal stress at 371°C was assumed to be zero. The thermal stress at a temperature (T) in a cross-ply region was calculated by integrating equation (2) from T to 371°C. The stress values at −54°C and 232°C are shown in Figure 2(b) (black solid line) with the temperature profile of cycles (Figure 2(a)).

Numerical calculation of thermal stress in T650-35 8HS/PMR-15 composites revealed that the thermal stress in the crimped region was 12% greater than in the cross-ply region.⁷ Because PMR-15 and TriA X exhibited similar thermal expansion behavior, T650-35 8HS/TriA X laminates are expected to exhibit thermal stress distribution similar to T650-35 8HS/PMR-15. Thus, thermal stress in crimped regions of T650-35 8HS/TriA X laminates was estimated by multiplying the calculated stress in the cross-ply region by 12%, shown as the black dashed line in Figure 2(b).

The goal of thermal stress calculation is to demonstrate the thermal stress level relative to the matrix strength. The tensile strength of neat TriA X was measured at −54°C and 232°C,¹⁵ and results are shown as the blue line in Figure 2(b). The internal stress induced by thermal cycles is 51% and 60% less than the tensile strength of the matrix at −54°C and 232°C, respectively. Thus, T650-35 8HS composites were expected to exhibit resistance to microcracking during thermal cycling between these temperatures (−54°C and 232°C).

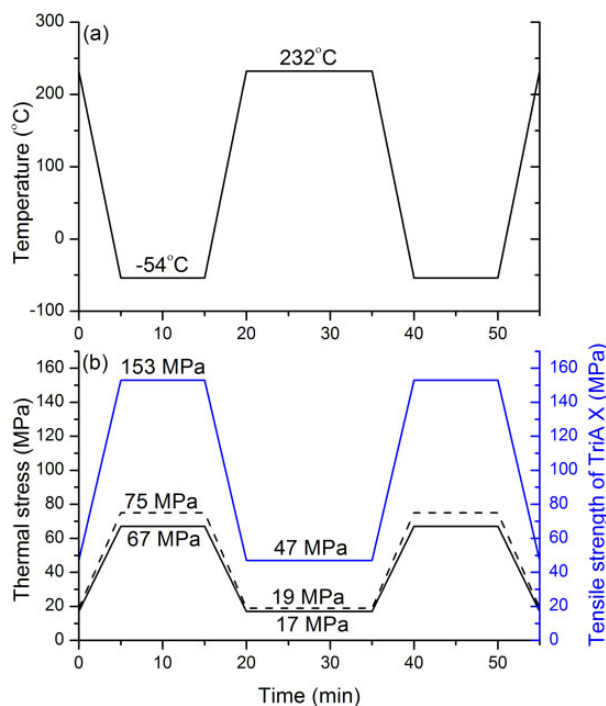


Figure 2. (a) Temperature profile of thermal cycles and (b) corresponding thermal stress in cross-ply region (solid black) and crimped region (dashed black) of $[0]_8$ laminates and tensile strength of the matrix¹⁵ (blue).

Thermal cycling experiments

Materials

TriA X prepreg was fabricated using an 80-wt% PMDA diester/p-ODA/PEPA monoester solution in ethanol, which was combined with desized T650-35/8HS/3 K carbon fabric (areal weight: 368 g m^{-2} , Cytec Solvay Group, Anaheim, CA, USA), yielding a fiber volume fraction of 55% after cure. T650-35 8HS/TriA X composites were fabricated in two layup sequences— $[0]_8$ and $[0/+45/-45/90]_8$ —using a molding cycle described previously.¹⁹ A TriA X neat polymer panel was prepared by molding PMDA diester/p-ODA/PEPA monoester powder blend in a hot press.¹⁵

Thermal cycling conditions

8HS laminates were machined into rectangular coupons for thermal cycling followed by microcrack inspection and SBS testing. Specimen dimensions are described in subsequent sections (*Microcrack inspection* and *SBS test*). Neat polymer coupons ($40 \times 40 \times 3 \text{ mm}^3$) were prepared for investigation of effects of thermal cycling on matrix physical properties. Thermal cycling test specimens were wet machined, then dried at 100°C for 64–89 h and stored in desiccators prior to thermal cycling. The specimens were thermally cycled between -54°C and 232°C with a 10-min

hold at -54°C and a 15-min hold at 232°C (Figure 2(a)). Up to 2000 thermal cycles were performed at The Boeing Company, Huntington Beach. Samples were removed every 400 cycles for microcrack inspection and testing.

Microcrack inspection

Composite specimens ($100 \times 50 \times 3 \text{ mm}^3$) with both layup sequences were inspected for microcracks at 400-cycle intervals, and SBS tests were performed. Each specimen was sectioned in three orientations— 0° (warp), 45° , and 90° (fill)—and mounted in potting resin. The cross sections (approximately 20 mm long) were wet polished down to $1 \mu\text{m}$ diamond suspension and inspected for microcracks using a digital microscope (VHX-600, Keyence, Japan).

High-resolution X-ray tomography (micro computed tomography (micro-CT)) was performed on the composite specimens before thermal cycling and after 2000 cycles to detect microcracks in three dimensions. Specimens were sectioned from thermally cycled laminates and scanned (XT H 225ST, Nikon, Japan). Mo- K_α incident radiation ($\lambda = 0.71 \text{ \AA}$) was used with 60 kV/220 μA voltage/intensity settings to achieve a resolution of $\leq 4 \mu\text{m}$ per pixel.

Oxidized layer inspection

A 2-mm-thick cross section ($6 \times 3 \text{ mm}^2$) was cut from the neat polymer specimen after 2000 cycles. The cross section was wet polished on both sides down to $200 \mu\text{m}$ using a disc grinder and sandpapers. The cross section under transmitted light was imaged using a digital microscope (VHX-600, Keyence) to detect discoloration from oxidation.

Dynamic mechanical analysis

Dynamic mechanical analysis was performed to determine T_g values of T650-35 8HS laminates and neat polymer before and after thermal cycling (Q800, TA Instruments). The measurements were carried out in single cantilever mode at a heating rate of 5°C min^{-1} with a fixed frequency of 1 Hz and a strain of 0.3%. The peak of the $\tan \delta$ curve was recorded to determine T_g .

Nanoindentation

Nanoindentation was conducted on neat polymer samples before and after thermal cycling to measure the surface Young's modulus. The indentation was carried out using continuous stiffness measurement mode with a constant strain rate of 0.01 s^{-1} at an oscillation frequency of 45 Hz, using a nano-indenter (Nano Indenter XP, MTS, Eden Prairie, MN, USA) with a Berkovich tip (TB26980, Keysight Technologies, Santa Rosa, CA, USA). The maximum penetration depth was 2000 nm, and drift correction was applied during tests. Fifty indents were performed on

Table 2. Specimens for SBS tests.

Number of cycles	Layup sequence							
	[0/+45/−45/90] _s				[0] ₈			
	Length (mm)	Width (mm)	Thickness (mm)	Number of specimens	Length (mm)	Width (mm)	Thickness (mm)	Number of specimens
0	18.64	6.20	3.10	8	18.41	6.13	3.08	5
400	18.66	6.21	3.12	6	18.41	6.13	3.11	5
800	18.66	6.21	3.09	7	18.41	6.11	3.08	5
1200	18.65	6.19	3.12	8	18.41	6.12	3.09	8
1600	18.63	6.20	3.10	8	18.42	6.13	3.10	5
2000	18.66	6.21	3.12	8	18.41	6.12	3.09	5

SBS: short-beam shear.

each specimen with an indentation spacing of $> 100 \mu\text{m}$. Young's modulus was calculated as the average result between 600 nm and 1000 nm using analysis software (TestWorks 4, MTS).

SBS test

The SBS strength of T650-35 8HS/TriA X composites was measured at room temperature in accordance with ASTM D2344.²⁰ Specimen thermal history, dimension, layup sequence, and number are summarized in Table 2. The tests were performed on a load frame (5567, Instron, Norwood, MA, USA) at a crosshead displacement rate of 1.0 mm min^{-1} . Specimens were stored in desiccators for at least 7 days prior to testing. After testing, polished sections were inspected to determine failure modes using a digital microscope (VHX-600, Keyence). Only interlaminar shear failures were observed (Online Supplemental Figure S1).

Results and discussion

Microcrack inspection

Composite specimens were removed from the thermal cycle chamber every 400 cycles for microcrack inspection. Specimens were sectioned and polished in three orientations (0° , 45° , and 90°) for observation. Figure 3 shows the polished sections of specimens after 2000 thermal cycles. No microcracks were observed in any of the specimens using light microscopy. For further inspection, micro-CT scans were performed on specimens after 2000 thermal cycles. Only a few microcracks were observed, and the morphology and position of microcracks (relative to the fabric architecture) were similar for all the cracks observed. Figure 4 shows a typical microcrack (outlined in red rectangles), where the image sequence extends from one end of a microcrack (a) to the other end (h). The sequence is also represented schematically in Figure 5, which shows the three-dimensional distribution of microcracks, using color to indicate the layer position of microcracks. For

example, yellow lines depict microcracks located in the first ply of the laminate.

Microcracking was detected only in the resin-rich regions near tow crimp of 8HS laminates (Figure 4). In these laminates (Figure 4(i)), three types of fiber regions are present: a cross-ply region (III), two tow edges (I and II) at an overlap of orthogonal tows, and a crimp region (I–II). In Figure 4(a), tow A was at a tow edge (I_A) of a tow overlap region, while tow B was in a cross-ply region (III_B) that was near a crimp. A microcrack terminated in the resin-rich region adjacent to tow A (Figure 4(b)). In Figure 4(c) and (d), tow A extended into the cross-ply region (III_A) that was yet close to the crimp, while tow B reached the first tow edge (I_B) of a tow overlap, where the resin-rich region was larger and the microcrack spanned the entire region. In Figure 4(e) and (f), tow B was situated at the tow overlap (I–II_B) and the microcrack was at a boundary between tow A and an adjacent fiber tow. In Figure 4(g), tow B reached the second tow edge (II_B) of the tow overlap, and the resin-rich region around the microcrack became smaller so that the microcrack was shorter. In Figure 4(h), both tow A and tow B were in the cross-ply region, and the microcrack had terminated. The microcrack shown in Figure 4 is typical of all microcracks observed in the micro-CT scans of the 8HS laminates X. The full set of micro-CT scans of the microcrack presented in Figure 4 is shown as a video in Online Supplemental Material and available at <https://youtu.be/cuwALxuYroU>.

The features of the microcracks in the micro-CT scans of thermally cycled laminates differed from those of thermal-cycling-induced microcracks in polyimide composites. As described above, microcracking was observed only in the resin-rich regions of laminates and was attributed to matrix failure. In contrast, microcracking in other polyimide composites typically occurred within fiber tows (fiber-rich regions), stemming from debonding at fiber–matrix interfaces.^{8,10–13} In addition to this difference in microcrack location, the distribution of microcracks in T650-35 8HS/TriA X was inconsistent with that of the

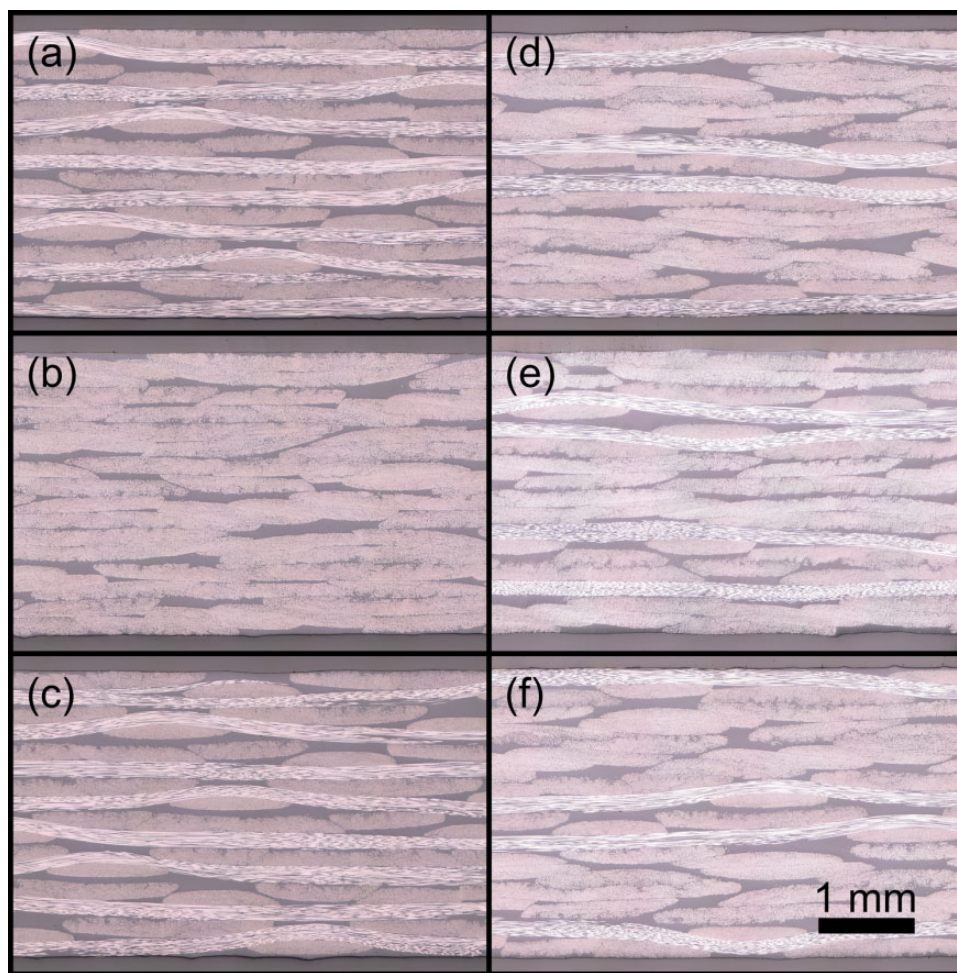


Figure 3. 8HS laminates after 2000 cycles: $[0]_8$ in 0° (a), 45° (b), and 90° (c), and $[0/+45/-45/90]_s$ in 0° (d), 45° (e), and 90° (f). 8HS: 8-harness satin.

typical microcracking generated by temperature variations. All microcracks occurred in one fiber direction in each laminate, apart from just two microcracks in $\pm 45^\circ$ plies of the $[0/+45/-45/90]_s$ layup. Because of the woven reinforcement, microcracks caused by internal stress are expected to appear in both fill and warp directions (based on accepted microcracking mechanics). Moreover, the microcracks here appeared only on one side of the specimens, while thermal cycling-induced microcracks normally occur in all fiber directions and are distributed symmetrically with respect to laminate midplanes.^{8,10,13}

The unusual features of the microcracks observed in the micro-CT scans indicate that factors other than thermal cycling were responsible for the cracks. The characteristics of the microcracks were consistent with artifactual damage. In particular, the micro-CT specimens were machined using a low-speed diamond saw after thermal cycling. Cyclic bending loads were applied to the specimens during sectioning, producing microcracks, of which approximately 50% were near to the cut surfaces. Based on

comparison of microcracks in the 8HS laminates and thermal-cycling-induced microcracks reported in other polyimide composites,^{8,10-13} we concluded that the additional loading generated by sectioning after thermal cycling was the cause of the observed microcracking.

The microcracking observed in 8HS laminates (attributed to sectioning after thermal cycling) indicates that the matrix was embrittled by exposure to cyclic temperatures. Thus, thermal cycling was indirectly associated with the microcracking. Micro-CT scans were also performed on fresh specimens (machined by the same method as described above), and no microcracks were detected. During thermal cycling, three possible processes were involved. Because samples were thermally cycled in air, thermal oxidative aging was possible, causing matrix degradation.²¹ In addition, thermally driven fatigue and creep (at high temperatures) were possible because of the cyclic stress induced by temperature change. Both fatigue and creep can induce a process of defect nucleation before cracking occurs, leading to rupture of atomic bonds and

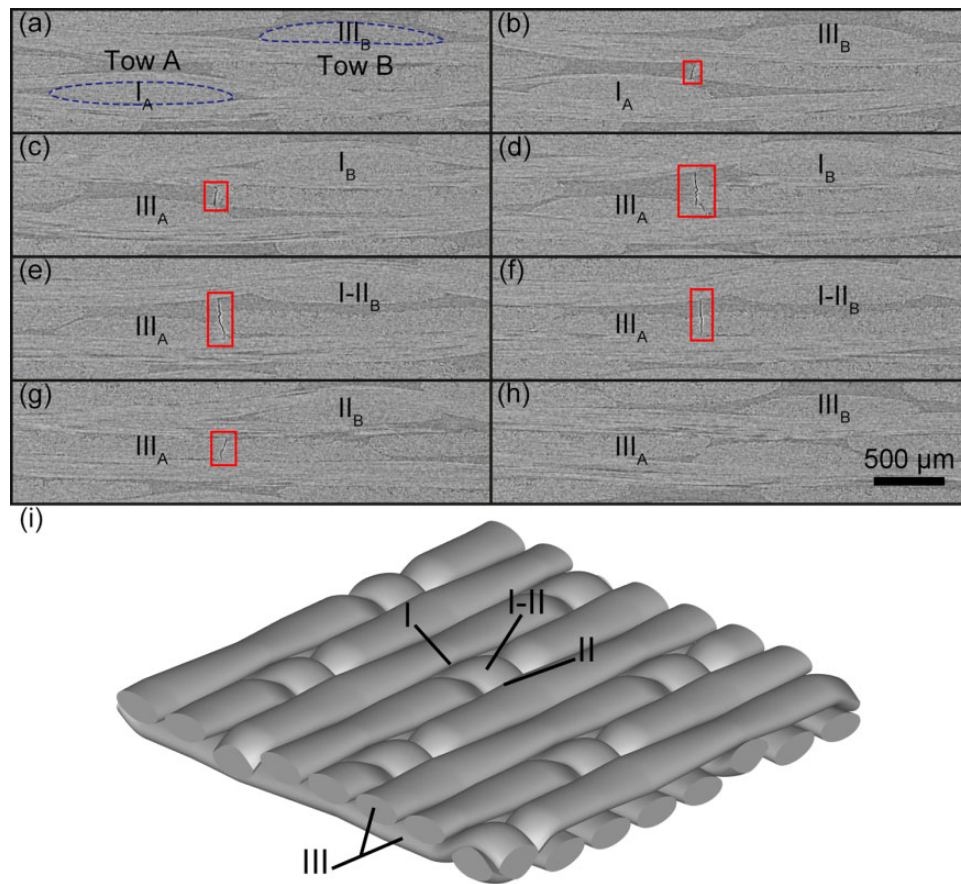


Figure 4. A typical microcrack (boxed in red rectangles) observed in micro-CT scans of 8HS laminates after 2000 cycles; image sequence from (a) to (h) is corresponding to direction from (a) to (h) indicated in Figure 5; (i) fiber morphology in 8HS weave: tow edges (I and II) at an overlap of orthogonal tows (I-II) and cross-ply region (III). 8HS: 8-harness satin; CT: computed tomography.

creating stress concentration sites in forms of chain ends and cavities (clusters of ruptured bonds).^{22,23} Any increase in defects generated by fatigue and creep could result in greater brittleness of the matrix and make microcracking easier upon additional loading afterward. The effects of these three factors are discussed next.

Effects on matrix

Thermal oxidation of polyimides commonly manifests as surface discoloration and increased T_g and Young's modulus.^{24–27} To investigate the effects of thermal oxidative aging on the matrix during thermal cycling, neat polymer specimens were thermally cycled in the same conditions with the composite specimens. Thermal stress was induced by fiber–matrix interaction upon temperature change. When the fibers were absent in the system, no thermal stress occurred. Note that the neat polymer specimens were the same thickness (3 mm) as the composite specimens, giving similar through-thickness temperature gradients during heating and cooling. Thus, the neat TriA X specimens experienced nearly identical thermal/oxidative exposure to the composites, but without thermal stress.

A thin section of neat polymer after 2000 cycles is shown in Figure 6, imaged with transmitted light, showing no discolored surface layer (the curved profile at corners was created by the saw kerf). Discoloration caused by thermal oxidation has been widely reported for PMR-15,^{24,25,27} and this has also been reported in long-term thermal oxidative aging of TriA X at 288°C. The T_g and Young's modulus (measured on the surface) of neat polymer after thermal cycling are summarized in Figure 7. The T_g and Young's modulus exhibited negligible change (approximately 1%) after 2000 cycles. Oxidized polymers typically exhibit greater Young's modulus than fresh polymers, and this is commonly observed in PMR-15 and other thermosets.^{24,27,28} The constant physical properties of neat TriA X after thermal cycling indicate that no thermal oxidative degradation occurred in the matrix of 8HS laminates during 2000 thermal cycling. As discussed in *Microcrack Inspection*, only three factors, thermal oxidative aging, thermally driven fatigue, and creep, could degrade the matrix in thermal cycling test and reduce the microcracking resistance upon additional loading. Because thermal oxidative aging was excluded, the other

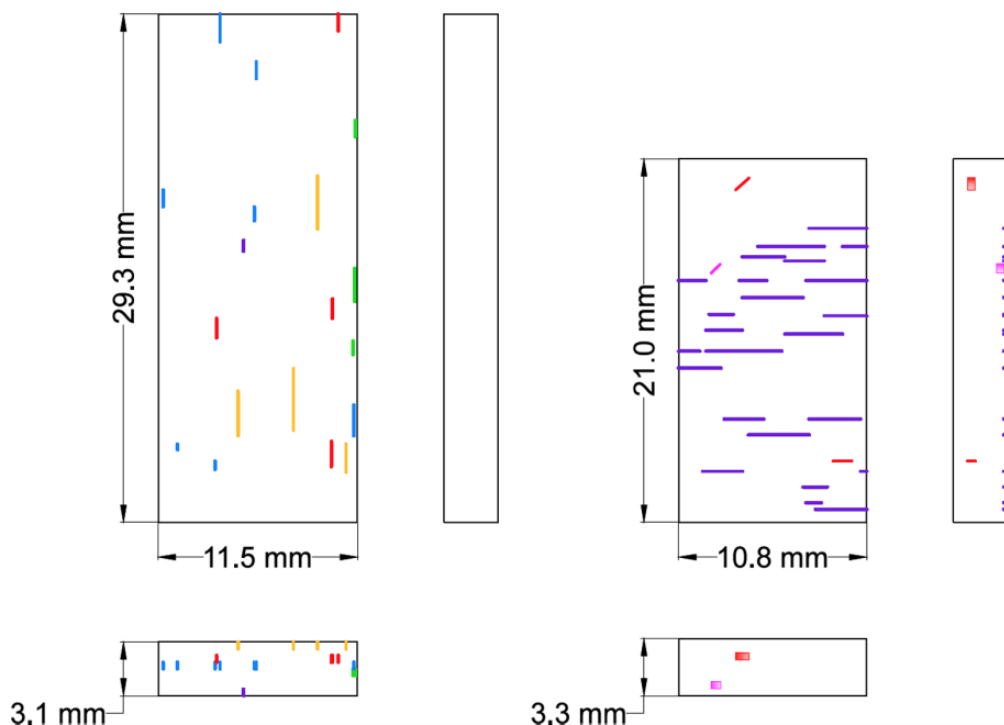


Figure 5. Microcrack distribution observed in micro-CT scans of T650-35 8HS/TriA X after 2000 cycles; color indicates ply position of microcracks. 8HS: 8-harness satin; CT: computed tomography.

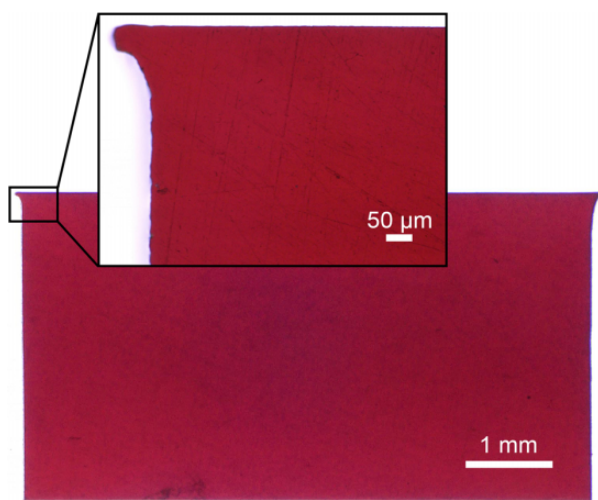


Figure 6. Cross section of neat TriA X after 2000 cycles (transmitted light).

two factors, thermally driven fatigue and creep, likely caused the matrix degradation.

To determine the effects of thermally driven fatigue and creep on the matrix of T650-35 8HS/TriA X, matrix-dominated properties— T_g and SBS strength—were measured (Figure 8). T_g (red solid triangles and green solid diamonds in Figure 8) exhibited negligible change (0.3–0.4% decrease) after 2000 cycles, while the SBS strength of $[0]_8$ (red solid squares in Figure 8) and $[0/+45/-45/90]_s$

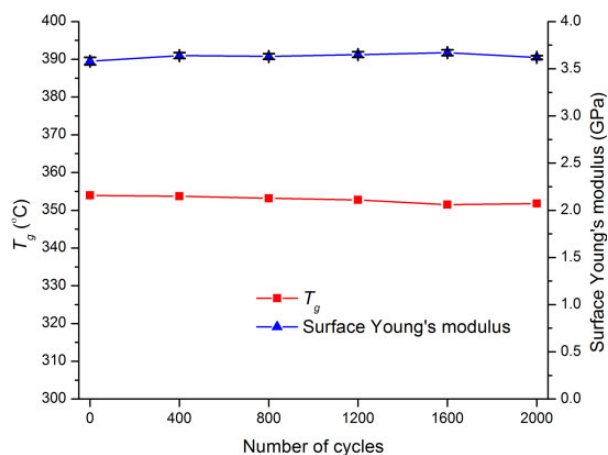


Figure 7. T_g and Young's modulus at surface of neat TriA X.

(blue solid circles in Figure 8) decreased slightly, by 3.3% and 9.1%, respectively. Because SBS strength is a matrix-dominated property, the decrease in SBS strength indicates mechanical degradation of the matrix. As described above, only local fatigue and creep induced by cyclic temperatures contribute to matrix degradation. To determine the relative importance of these factors, SBS tests were performed on specimens aged for 500 h at 232 C, equivalent to the total time at 232 C during 2000 cycles. During aging at 232 C, only local creep could affect the composites, because the thermal stress was constant at constant temperature. The

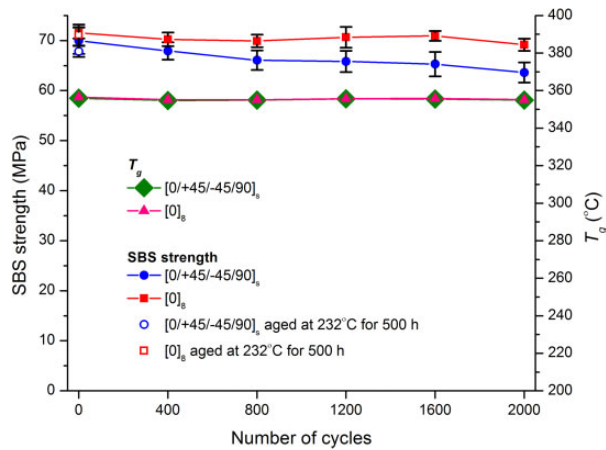


Figure 8. T_g and SBS strength of T650-35 8HS/TriA X. SBS: short-beam shear.

SBS strength of aged $[0]_8$ (red hollow square in Figure 8) and $[0/+45/-45/90]_s$ (blue hollow circle in Figure 8) laminates was 0.6% and 3.1% less than that of fresh specimens, respectively, and can be attributed to possible local creep or normal measurement variance. The slight decreases in SBS cannot prove the existence of creep or exclude the possibility. However, the effects of local creep are negligible or secondary in comparison to thermal fatigue, because the SBS strength reduction after isothermal aging was far less (82% less for $[0]_8$ laminates and 67% less for $[0/+45/-45/90]_s$ laminates) than after 2000 thermal cycles, where both fatigue and creep could have occurred. Therefore, thermally driven fatigue is identified as the primary factor responsible for mechanical degradation of the matrix, resulting in the reduction in SBS strength after thermal cycling, while creep at high temperatures is possibly a secondary factor. The slightly greater (6%) SBS strength retention observed in the thermally cycled $[0]_8$ laminates compared to $[0/+45/-45/90]_s$ laminates is attributed to effects of layup sequences—the SBS strength of isotropic layups is more matrix-controlled than that of cross-ply layups.⁸

In addition to thermally driven fatigue and creep, fabric geometry also affected the mechanical degradation of the matrix. The resin-rich regions were adjacent to crimped tows in the 8HS laminates. The thermal stress in the crimped region is 12% greater than that in the cross-ply region because of the tow curvature.⁷ Thus, resin pockets in crimped regions sustain maximum thermal stress. Here, no fiber reinforcement was present to carry the thermal stress, and thus crimped regions were most susceptible to thermal cycling damage. Consequently, microcracking occurred upon addition loading. To increase microcracking resistance after thermal cycling, fabric architecture that minimizes/eliminates fiber crimp will mitigate effects of resin-rich regions. Thus, nonwoven reinforcement, such as non-crimp

fabric, unidirectional tape, or spread-tow fabric, should impart increased resistance to thermal cycling degradation.

Although the matrix degraded slightly from thermal cycling, the retention of SBS strength was greater than 90% after 2000 cycles. Fiber-dominated mechanical properties are not as sensitive to microcracks as matrix-dominated properties.^{8,10} SBS strength (interlaminar shear strength) is one of the common matrix-dominated properties investigated as an indicator of mechanical performance in thermal cycling tests of polyimide composites.¹ Note that the interlaminar shear strength of PMR-15 composites after 1500 cycles between -55°C and 232°C was reported to be approximately 40% of the initial value because of extensive microcracking, which arose from the low transverse tensile strength of laminae (comparable to the predicted thermal stress level).¹¹ In contrast, high residual matrix-dominated properties of TriA X are attributed to the absence of microcracks, which in turn stemmed from the high tensile strength of the matrix.

Conclusions

Resistance to microcracking during thermal cycling is a critical performance indicator for polyimide composites because of the brittle nature and high CTE of the matrix. Indeed, no polyimide composites have been reported to date that withstand thermal cycling (with similar temperature ranges) without microcracking. Unlike conventional polyimides, TriA X possesses greater tensile strength, sufficient to withstand the thermal stresses induced by cyclic temperatures. As reported previously, the intrinsic strength stems from the distinctive molecular structure. Conventional image analysis did not reveal microcracks in thermally cycled laminates, although a few microcracks were detected in micro-CT scans. These cracks were attributed to additional loading during sample sectioning subsequent to thermal cycling. The >90% retention of SBS strength after 2000 cycles was attributed to the absence of microcracks in the specimens, while the <10% reduction was attributed to slight matrix degradation. After 2000 cycles, laminates were more susceptible to damage from sectioning than from interlaminar shear loading. Additional investigation is needed to more fully understand the mechanical behavior of TriA X composites after thermal cycling.

Three factors—thermal oxidative aging, thermally driven fatigue, and creep—were considered as possible causes of the SBS strength degradation, and two of these were deemed unlikely. First, no evidence of thermal oxidation from thermal cycling was detected. Thermally driven fatigue induced by the cyclic temperatures is the primary cause of the mechanical degradation of the matrix, while creep is the possible secondary factor. In addition to local fatigue and creep, curved fiber geometry of 8HS fabric also affected the performance of the matrix and decreased the microcracking resistance of the composites after thermal

cycling. Thus, nonwoven reinforcement is recommended for TriA X composites in future work.

In the field of polyimide composites, PMR-15 has been the most widely reported matrix for high-temperature applications. However, all polyimide composites, including PMR-15 composites, undergo extensive microcracking during thermal cycling, which is a major limitation, particularly for oxidizing environments. Thus, polyimide composites are limited presently to short-term structural components or long-term nonstructural components.¹⁰ The results presented here demonstrate that composites based on a newly designed polyimide (TriA X) can withstand thermal cycling without microcracking. The increased resistance to thermal cycling is likely to expand the design space of polyimide composites for longer term high-temperature structural applications.

Author note

William Guzman of Kaneka Americas Holding, Inc. prepared TriA X monomeric resin, and Sidharth Sarojini Narayan and William Edwards of University of Southern California performed microscopic imaging and micro-CT analysis, respectively.

Acknowledgments

The authors thank Dr Timotei Centea of USC for advice in manuscript preparation and Dr Thomas Tsotsis of the Boeing Company for thermal cycling tests. The authors also acknowledge Kaneka Americas Holding, Inc for financial support.



Declaration of conflicting interests

The author(s) declared no potential conflicts of interest with respect to the research, authorship, and/or publication of this article.

Funding

The author(s) disclosed receipt of the following financial support for the research, authorship, and/or publication of this article: This work was supported by Kaneka Corporation and Kaneka Americas Holding, Inc.

ORCID iD

Yixiang Zhang  <https://orcid.org/0000-0003-3325-1730>
Steven Nutt  <https://orcid.org/0000-0001-9877-1978>

Supplemental material

Supplemental material for this article is available online.

References

1. Hancox N. Thermal effects on polymer matrix composites: part 1. Thermal cycling. *Mater Des* 1998; **19**(3): 85–91.
2. Naebe M, Abolhasani MM, Khayyam H, et al. Crack damage in polymers and composites: a review. *Polym Rev* 2016; **56**(1): 31–69.
3. Kravchenko OG, Kravchenko SG and Pipes RB. Chemical and thermal shrinkage in thermosetting prepreg. *Compos A Appl Sci Manuf* 2016; **80**:72–81.
4. Khoun L and Hubert P. Investigation of the dimensional stability of carbon epoxy cylinders manufactured by resin transfer moulding. *Compos A Appl Sci Manuf* 2010; **41**(1): 116–124.
5. White SR and Hahn H. Process modeling of composite materials: residual stress development during cure. Part II. Experimental validation. *J Compos Mater* 1992; **26**(16): 2423–2453.
6. Takagaki K, Hisada S, Minakuchi S, et al. Process improvement for out-of-autoclave prepreg curing supported by in-situ strain monitoring. *J Compos Mater* 2017; **51**(9): 1225–1237.
7. Rupnowski P and Kumosa M. Meso- and micro-stress analyses in an 8HS graphite/polyimide woven composite subjected to biaxial in-plane loads at room temperature. *Compos Sci Technol* 2003; **63**(6): 785–799.
8. Tompkins S and Williams SL. Effects of thermal cycling on mechanical properties of graphite polyimide. *J Space Rocket* 1984; **21**(3): 274–280.
9. Dato MH. *Mechanics of fibrous composites*. London, UK: Elsevier Science, 1991.
10. Owens G and Schofield S. Thermal cycling and mechanical property assessment of carbon fibre fabric reinforced PMR-15 polyimide laminates. *Compos Sci Technol* 1988; **33**(3): 177–190.
11. Wilson D, Wells J, Hay J, et al. Preliminary investigations into the microcracking of PMR-15/graphite composites. I. Effect of cure temperature. *SAMPE J*. 1987; **23**:35–42.
12. Gentz M, Armentrout D, Rupnowski P, et al. In-plane shear testing of medium and high modulus woven graphite fiber reinforced/polyimide composites. *Compos Sci Technol* 2004; **64**(2): 203–220.
13. Shimokawa T, Katoh H, Hamaguchi Y, et al. Effect of thermal cycling on microcracking and strength degradation of high-temperature polymer composite materials for use in next-generation SST structures. *J Compos Mater* 2002; **36**(7): 885–895.
14. National Research Council. *US supersonic commercial aircraft: assessing NASA's high speed research program*. Washington, DC: National Academies Press, 1997, p. 72.
15. Zhang Y, Miyauchi M and Nutt S. Structure and properties of a phenylethynyl-terminated PMDA-type asymmetric polyimide. *High Perform Polym* 2018. DOI: 10.1177/0954008318762592.
16. Benedikt B, Kumosa M, Predecki P, et al. An analysis of residual thermal stresses in a unidirectional graphite/PMR-15 composite based on X-ray diffraction measurements. *Compos Sci Technol* 2001; **61**(14): 1977–1994.
17. ASTM E2113. *Standard test method for length change calibration of thermomechanical analyzers*. West Conshohocken: ASTM International, 2013.
18. ASTM E831. *Standard test method for linear thermal expansion of solid materials by thermomechanical analysis*. West Conshohocken: ASTM International, 2014.

19. Zhang Y, Jain A, Grunenfelder LK, et al. Process development for phenylethynyl-terminated PMDA-type asymmetric polyimide composites. *High Perform Polym* 2018; **30**(6): 731–741.
20. ASTM D2344. *Standard test method for short-beam strength of polymer matrix composite materials and their laminates*. West Conshohocken: ASTM International, 2016.
21. Lafarie-Frenot M and Rouquie S. Influence of oxidative environments on damage in c/epoxy laminates subjected to thermal cycling. *Compos Sci Technol* 2004; **64**(10–11): 1725–1735.
22. Sauer J and Richardson G. Fatigue of polymers. *Int J Fract* 1980; **16**(6):499–532.
23. Vujosevic M and Krajcinovic D. Creep rupture of polymers—a statistical model. *Int J Solids Struct* 1997; **34**(9): 1105–1122.
24. Johnson LL, Eby R and Meador MAB. Investigation of oxidation profile in PMR-15 polyimide using atomic force microscope (AFM). *Polymer* 2003; **44**(1): 187–197.
25. Tandon G, Pochiraju K and Schoeppner G. Thermo-oxidative behavior of high-temperature PMR-15 resin and composites. *Mater Sci Eng A* 2008; **498**(1–2): 150–161.
26. Scola D and Vontell J. Mechanical properties and mechanism of the degradation process of 316°C isothermally aged graphite fiber/PMR-15 composites. *Polym Eng Sci* 1991; **31**(1): 6–13.
27. Lu Y, Tandon G, Putthanarat S, et al. Nanoindentation strain rate sensitivity of thermo-oxidized PMR-15 polyimide. *J Mater Sci* 2009; **44**(8): 2119–2127.
28. Barjasteh E, Bosze E, Tsai Y, et al. Thermal aging of fiber-glass/carbon-fiber hybrid composites. *Compos A Appl Sci Manuf* 2009; **40**(12): 2038–2045.